Cell Reports
Article

Cracking the Molecular Origin of Intrinsic Tyrosine Kinase Activity through Analysis of Pathogenic Gain-of-Function Mutations

Huaibin Chen,[1,3,7] Zhifeng Huang,[1,3,7] Kaushik Dutta,[4,7] Steven Blais,[2] Thomas A. Neubert,[1,2] Xiaokun Li,[3] David Cowburn,[5] Nathaniel J. Traaseth,[6] and Moosa Mohammadi[1,*]
[1]Department of Biochemistry and Molecular Pharmacology, New York University School of Medicine, New York, NY 10016, USA
[2]Kimmel Center for Biology and Medicine at the Skirball Institute, New York University School of Medicine, New York, NY 10016, USA
[3]School of Pharmacy, Wenzhou Medical College, Wenzhou, Zhejiang 325035, China
[4]New York Structural Biology Center, New York, NY 10027, USA
[5]Department of Biochemistry, Albert Einstein College of Medicine, Yeshiva University, Bronx, NY 10461, USA
[6]Department of Chemistry, New York University, New York, NY 10003, USA
[7]These authors contributed equally to this work
*Correspondence: moosa.mohammadi@nyumc.org
http://dx.doi.org/10.1016/j.celrep.2013.06.025

SUMMARY

The basal (ligand-independent) kinase activity of receptor tyrosine kinases (RTKs) promotes *trans*-phosphorylation on activation loop tyrosines upon ligand-induced receptor dimerization, thus upregulating intrinsic kinase activity and triggering intracellular signaling. To understand the molecular determinants of intrinsic kinase activity, we used X-ray crystallography and NMR spectroscopy to analyze pathogenic FGF receptor mutants with gradations in gain-of-function activity. These structural analyses revealed a "two-state" dynamic equilibrium model whereby the kinase toggles between an "inhibited," structurally rigid ground state and a more dynamic and heterogeneous active state. The pathogenic mutations have different abilities to shift this equilibrium toward the active state. The increase in the fractional population of FGF receptors in the active state correlates with the degree of gain-of-function activity and clinical severity. Our data demonstrate that the fractional population of RTKs in the active state determines intrinsic kinase activity and underscore how a slight increase in the active population of kinases can have grave consequences for human health.

INTRODUCTION

Receptor tyrosine kinases (RTKs) regulate a myriad of biological processes in mammalian development, tissue homeostasis, and metabolism (Hunter, 2000; Lemmon and Schlessinger, 2010). At basal state, RTKs possess low levels of intrinsic kinase activity. This basal activity plays a key role in RTK signal transduction because it primes *trans*-phosphorylation of tyrosines in the activation loop (A loop) upon ligand binding and receptor dimerization resulting in full activation of the kinase. This in turn allows tyrosine phosphorylation of the kinase insert and flanking juxtamembrane and C-terminal tail regions of the RTKs. These secondary phosphorylation events then serve to recruit downstream signaling substrates for tyrosine phosphorylation by the activated RTK, culminating in activation of intracellular signaling pathways.

The basal, intrinsic activity of RTKs must be carefully balanced. Insufficient basal activity would diminish the ability of ligand-induced dimerization to promote A loop tyrosine *trans*-phosphorylation, and hence, signal transmission would stall. Conversely, excess basal activity would bypass the requirement for ligand-induced dimerization in kinase activation, resulting in ligand-independent constitutive RTK signaling. Indeed, kinase domain mutations that elevate or reduce the intrinsic activity of RTKs are common culprits in a diverse array of human diseases. An accumulated wealth of structural and biophysical data has revealed some insight into the autoinhibitory mechanisms that keep tyrosine kinase activity at bay (Hubbard, 2002) and has also elucidated the molecular basis of kinase activation by A loop tyrosine phosphorylation (Chen et al., 2007; Hubbard and Till, 2000; Pellicena and Kuriyan, 2006; Rajakulendran and Sicheri, 2010). Despite these major strides in understanding the mechanisms of kinase regulation, a fundamental question has remained unanswered: what precisely determines basal, intrinsic kinase activity?

In FGFR2 and FGFR3, a conserved lysine located two residues away from the A loop tyrosines is a major hot spot codon for pathogenic mutations. Substitutions of Lys650 in FGFR3 with Thr, Asn, Gln, Met, or Glu cause dwarfism syndromes of varying clinical severity (Vajo et al., 2000) (Figure S1). Among them, neonatal lethal thanatophoric dysplasia type II (TDII) is the most severe and is caused by the Lys650Glu mutation (Chen

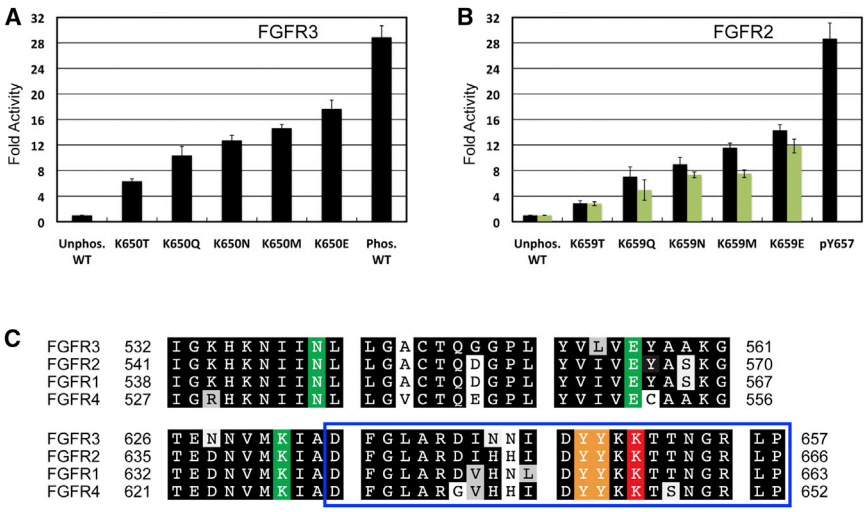

Figure 1. Pathogenic Mutations at Lys650 of FGFR3 Impart Different Degrees of A Loop Phosphorylation-Independent Kinase Activation

(A) Fold increase in the activity of Lys650 mutants and phosphorylated (Phos.) WT FGFR3 kinase over the unphosphorylated (Unphos.) WT FGFR3 kinase measured at 30 s. Error bars represent mean ± SD.

(B) Analogous mutations targeting Lys659 in FGFR2 kinase lead to a similar pattern of graded kinase activation. The activities of the pathogenic kinases are less than that of mono-phosphorylated FGFR2K^{pY657} (labeled as pY657), implying that the mutations activate in a partially ligand-independent fashion. Black and green bars represent Tyr656/Tyr657 and Phe656/Phe657 versions of the kinases, respectively. Error bars represent mean ± SD.

(C) Structure-based sequence alignment of the A loop and the autoinhibitory molecular brake among FGFR kinases. The A loop is boxed in blue. The twin tyrosines and the lysine on the A loop and the three components of the molecular brake are labeled in orange, red, and green, respectively. See also Figure S1.

et al., 2001; Tavormina et al., 1995; Webster et al., 1996; Wilcox et al., 1998). Substitution of Lys650 with Met causes severe achondroplasia with developmental delay and acanthosis nigricans (SADDAN) syndrome (Bellus et al., 1999; Tavormina et al., 1999). The Lys650Asn and Lys650Gln mutations lead to hypochondroplasia (HCH), a mild form of dwarfism (Bellus et al., 1995, 2000). The Lys650Thr mutation causes an even milder form of HCH (Berk et al., 2007; Castro-Feijóo et al., 2008). In vitro autophosphorylation assays have shown that these mutations confer different degrees of ligand-independent activation on FGFR kinase and that the degree of aberrant activation correlates with the clinical severity of the dwarfism syndromes caused by the mutations (Bellus et al., 2000). This naturally occurring set of pathogenic kinases with graded kinase activity provides a powerful tool to explore the molecular determinants of intrinsic kinase activity. In this report, we studied the impact of these five pathogenic mutations on the structure and dynamics of FGFR kinase using X-ray crystallography and NMR spectroscopy. Our data uncover a "two-state" dynamic equilibrium model for regulation of FGFR kinase and likely other RTKs and show that the fractional population of the kinase in the active state determines intrinsic kinase activity.

RESULTS AND DISCUSSION

Pathogenic Mutations of Lys650/Lys659 of FGFR3/FGFR2 Elevate Intrinsic Kinase Activity of FGFR Independent of A Loop Tyrosine Phosphorylation

Bellus and colleagues (Bellus et al., 2000) were the first to study the impact of the dwarfism syndrome mutations at Lys650 on the kinase activity of FGFR3 and noticed a functional-clinical correlation between the degree of gain of function and severity of skeletal phenotypes (Figure S1). In their study, wild-type (WT) full-length FGFR3 and its mutants harboring the pathogenic substitutions at Lys650 were overexpressed in mammalian cells, and the activities of immunopurified receptors were compared using an in vitro autophosphorylation assay. This approach has two limitations, however. First, due to the activating nature of these mutations, the overexpressed receptor mutants may contain residual A loop tyrosine phosphorylation, which would confound conclusions about the kinase assay data. Second, measuring intrinsic kinase activity using autophosphorylation can be potentially misleading because the mutations could affect the latter in the absence of an effect on kinase activity. To unambiguously determine the impact of the pathogenic mutations on the intrinsic kinase activity of FGFR3 kinase, we purified phosphorylation-free WT and mutated FGFR3 kinase domains and compared their intrinsic activities using a substrate phosphorylation assay. Our kinase assay data show that the mutations differentially enhance the intrinsic activity of FGFR3 kinase in the following order: Lys650Glu > Lys650Met > Lys650Asn ~ Lys650Gln > Lys650Thr (Figure 1A). This trend is generally in agreement with the data reported by Bellus and colleagues (Bellus et al., 2000) except that in this previous study, Lys650Met showed greater autophosphorylation activity than Lys650Glu, which is inconsistent with the clinical severity of the dwarfism syndromes caused by these mutations.

Having confirmed the gradation in gain of function imparted by the different pathogenic mutations, we next examined the structural basis of graded kinase activation by the pathogenic mutations. Because comprehensive structural studies of this scale require an abundant source of protein, we decided to use the highly homologous FGFR2 kinase as the "workhorse" for this study because it can be expressed at higher levels in *E. coli* than the FGFR3 kinase. FGFR2 and FGFR3 kinases share 82% overall sequence identity, with 86% identity within the A loop, and both are regulated by the FGFR-invariant molecular brake at the kinase hinge region (Chen et al., 2007) (Figure 1C). Indeed, Lys659 (corresponding to Lys650 in FGFR3) and molecular brake mutations in FGFR2 kinase lead to gain of function in

Table 1. X-Ray Data Collection and Refinement Statistics

Construct	K659E	K659M	K659N	K659Q	K659T
Data Collection					
Resolution (Å)[a]	50–2.6 (2.69–2.6)	50–2.3 (2.34–2.3)	50–2.4 (2.44–2.4)	50–2.3 (2.34–2.3)	50–1.85 (1.88–1.85)
Space group	P1	$P4_322$	C2	$P4_322$	C2
Unit cell parameter: a (Å)	70.584	73.852	278.634	73.785	278.508
Unit cell parameter: b (Å)	70.278	73.852	78.122	73.785	78.395
Unit cell parameter: c (Å)	85.499	310.716	72.791	313.749	73.197
Unit cell parameter: α (°)	92.39	90.00	90.00	90.00	90.00
Unit cell parameter: β (°)	112.19	90.00	101.90	90.00	101.02
Unit cell parameter: γ (°)	115.98	90.00	90.00	90.00	90.00
Content of the asymmetric unit	4	2	4	2	4
Number of measured reflections	147,245	1,028,351	453,471	258,430	453,556
Number of unique reflections	41,786	39,689	60,839	38,222	127,643
Data redundancy	3.5	25.9	7.5	6.8	3.6
Data completeness (%)[a]	97.1 (84.5)	99.8 (100.0)	99.4 (99.3)	96.6 (99.8)	96.4 (89.4)
R_{sym} (%)[a,b]	7.4 (33.2)	11.4 (49.8)	5.9 (41.7)	11.8 (35.5)	3.1 (31.9)
I/sig	24.5	43.6	50.8	33.6	45.0
Refinement					
R factor/R_{free}	18.0/26.1	18.0/21.8	20.6/26.1	18.6/23.7	22.1/24.9
Number of protein atoms	9,011	4,838	8,709	4,818	8,996
Number of nonprotein/solvent atoms	141	78	139	51	149
Number of solvent atoms	135	190	90	229	397
Rmsd bond length (Å)	0.014	0.008	0.009	0.008	0.007
Rmsd bond angle (°)	1.567	1.132	1.201	1.170	1.153
PDB ID	4J97	4J96	4J95	4J98	4J99

[a]Numbers in parentheses refer to the highest resolution shell.
[b]$R_{sym} = \sum|I - \langle I\rangle| / \sum I$, where I is the observed intensity of a reflection, and $\langle I\rangle$ is the average intensity of all the symmetry-related reflections.

craniosynostosis syndromes (Kan et al., 2002), endometrial cancer (Pollock et al., 2007), and cervical cancer (Dutt et al., 2008). As expected, our substrate phosphorylation assay data show that the corresponding mutations in FGFR2 kinase, namely Lys659Glu, Lys659Met, Lys659Asn, Lys659Gln, and Lys659Thr, behave similarly and impart graded kinase activation following the same order as determined for FGFR3 kinase (Figures 1A and 1B). Notably, the data also show that the intrinsic activities of the pathogenic FGFR2 kinases are lower than that of FGFR2 kinase activated by A loop phosphorylation ($FGFR2K^{pY657}$), indicating that these pathogenic mutations activate the kinase in a partially ligand-independent fashion. These "pathogenic" FGFR2 kinases were then crystallized in the presence of a non-hydrolyzable ATP analog (AMP-PCP) and $MgCl_2$, and their structures were determined. Data collection and refinement statistics are summarized in Table 1.

Comparison of the crystal structures of the pathogenic FGFR2 kinases with those of unphosphorylated and A loop phosphorylated WT FGFR2 kinases reveals that all five mutants adopt the same active conformation, reminiscent of the phosphorylated WT kinase (Figures 2A and 2B). In each structure, the side chain of the mutated residue makes novel contacts with nearby residues, thus locally stabilizing an active A loop conformation. The rearranged A loop engages in favorable intramolecular contacts with the αC helix in the N lobe leading to closer apposition of the N and C lobe and disengagement of the molecular brake at the kinase hinge region, which allows the kinase to adopt the active conformation. In the Lys659Met mutant structure, the side chain of Met659 binds a hydrophobic depression formed by Leu665, Met670, Ala674, Tyr680, and Tyr657, the latter of which is located in the A loop (Figure 2C). In the remaining four mutant structures (Figures 2D–2G), the side chains of the mutated residues engage in hydrogen bonding with Arg625 in the catalytic loop. Moreover, in each of these four structures, the oxygen atoms from the side chains of the mutated residues participate in oxygen-aromatic interactions with Tyr657 in the A loop. In all five mutant structures, Tyr657 occupies a position similar to the phosphorylated Tyr657 in the activated WT kinase structure and makes a direct hydrogen bond with Arg649, which further supports an active A loop conformation. These data unambiguously demonstrate that the pathogenic mutations simulate an activated A loop conformation (Figure 2B). To ensure that the mechanism of activation observed in the FGFR2 kinase mutant structures truly reflects the effect of the actual pathogenic FGFR3 kinase mutations, we have solved the crystal structure of FGFR3 kinase harboring the Lys650Glu mutation. Similar to the Lys659Glu FGFR2 kinase structure, the carboxylate side chain of Glu650 engages in hydrogen bonding with Arg616 in the catalytic loop, while simultaneously participating in oxygen-aromatic interactions with Tyr648. These intramolecular interactions result in

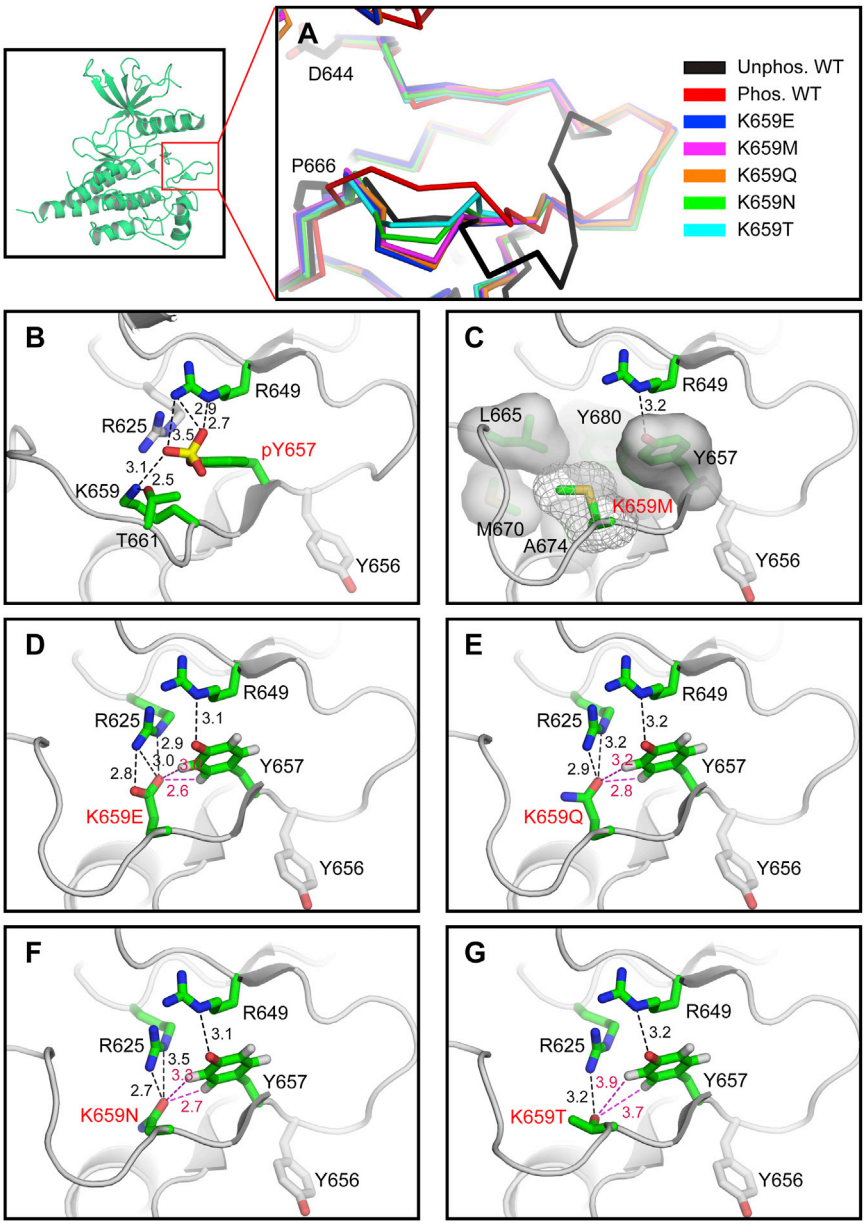

Figure 2. FGFR2 Kinase Lys659 Mutations Have Different Capacities to Stabilize the Active State Conformation of the A Loop

(A) Comparison of the A loop conformations of unphosphorylated WT (in black, PDB ID 2PSQ; Chen et al., 2007), phosphorylated WT (in red, PDB ID 2PVF; Chen et al., 2007), Lys659Glu mutant (in blue, PDB ID 4J97), Lys659Met mutant (in purple, PDB ID 4J96), Lys659Gln mutant (in orange, PDB ID 4J98), Lys659Asn mutant (in green, PDB ID 4J95), and Lsy659Thr mutant (in cyan, PDB ID 4J99) FGFR2 kinase structures. Asp644 and Pro666 lie at the beginning and end of the A loop and are indicated in the unphosphorylated WT kinase structure. The subtle difference in the C-terminal region of the A loop between the phosphorylated WT kinase and the unphosphorylated WT and mutant kinases is due to an interaction between this section of the A loop and substrate peptide (which is not present in any of the unphosphorylated WT and mutant kinase structures).

(B) Close-up view of intramolecular interactions introduced by A loop tyrosine phosphorylation (Chen et al., 2008).

(C–G) Close-up view of intramolecular interactions introduced by the Lys659 mutations. The mutant residues are labeled in red. Side chains of selected residues are shown as sticks. Atom colorings are as follows: oxygens are in red, nitrogens in blue, phosphorus in yellow, and carbons in green. The hydrogen bonds and oxygen aromatic interactions are shown as dashed lines with distance (in Å) labeled alongside in black and red, respectively. The hydrophobic interactions are represented by semitransparent surfaces.

stabilization of the A loop in the active conformation (Z.H., H.C., and M.M., unpublished data). To validate the mechanism of activation observed in the crystal structures of FGFR2 kinase mutants, the effects of mutating A loop tyrosines (Tyr656 and Tyr657) to phenylalanine were studied. The data show that elimination of A loop tyrosine phosphorylation only modestly reduces the activity of the pathogenic kinases (Figure 1B), which is consistent with the direct involvement of Tyr657 in the stabilization of an A loop active conformation (Figures 2C–2G).

A Two-State Dynamic Equilibrium Model Underlies FGFR Kinase Regulation

The structural data showing that all five pathogenic mutations stabilize the same active conformation as A loop tyrosine phosphorylation does in the WT kinase are surprising given the differences in the intrinsic activity of the mutant kinases and the mono-phosphorylated FGFR2K^{pY657}. Close inspection of the intramolecular contacts introduced by the different pathogenic mutations, however, unveils the molecular basis for the observed gradations in kinase activity of the mutants. The analysis shows a direct correlation between the number and length of hydrogen bonds and oxygen-aromatic interactions that each mutation introduces (summarized in Table S1) and the degree of gain in intrinsic kinase activity imparted by that mutation. This is best illustrated by comparing the structures of the most active mutant (Lys659Glu, Figure 2D) and the least active mutant (Lys659Thr, Figure 2G). In the Lys659Glu structure, the carboxylate side chain of Glu659 introduces a total of three strong hydrogen bonds ($\leq$3 Å) with Arg625 and two oxygen-aromatic interactions ($\leq$3 Å) with Tyr657. In contrast, the Lys659Thr structure shows that Thr659 makes only a single weak hydrogen bond (>3 Å) with Arg625 and two oxygen-aromatic interactions (>3.5 Å) with Tyr657. Hence, these static crystallographic snapshots imply that the pathogenic mutations have different potentials to stabilize the same active conformation of the enzyme.

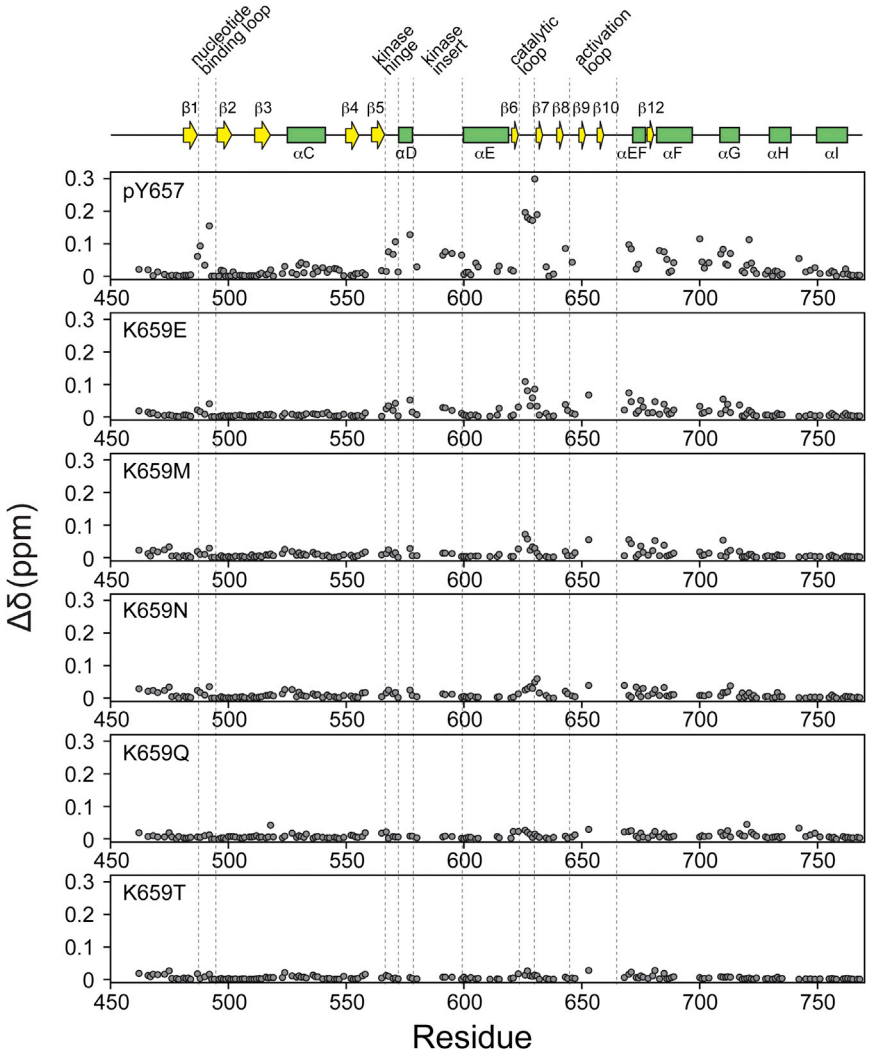

Figure 3. HSQC Chemical Shift Perturbation Plotted as a Function of Residue for the Mutants and the Mono-Phosphorylated FGFR2K^{pY657}

Δδ was calculated according to Equation 1 between the unphosphorylated WT kinase and the kinases indicated in the figure. These data were used to construct Figure S3.
See also Figures S2 and S3.

Taken together with the observed gradations in kinase activity, these X-ray crystallographic data led us to propose that FGFR kinase exists in dynamic exchange between an inhibited ground state conformation and an active state conformation and that the mutations act by increasing the population of kinase molecules in the active state. Accordingly, the fractional population of kinase molecules in the active state determines the intrinsic kinase activity.

To test this hypothesis, we employed NMR spectroscopy to investigate the effects of the mutations on the conformation and dynamics of FGFR2 kinase in solution. As expected, the overlay of HSQC spectra showed large chemical shift changes for many residues between unphosphorylated WT kinase and the mono-phosphorylated kinase, FGFR2K^{pY657} (Figure S2). Importantly, many residues in the kinase mutants also experienced chemical shift changes. Mapping of these perturbations onto the crystal structure of unphosphorylated WT FGFR2 kinase shows that the pathogenic mutations affected a similar set of residues as those perturbed by Tyr657 phosphorylation (Figures 3 and S3). Interestingly, several residues of the pathogenic kinases show chemical shifts that fall between those of the unphosphorylated WT kinase and the mono-phosphorylated FGFR2K^{pY657} along a straight, linear trajectory (Figures 4A and S4). Notably, the HSQC spectra for the unphosphorylated WT kinase and all five pathogenic mutant kinases contain a relatively narrow peak for each residue, indicating a fast chemical exchange with the two endpoints of the chemical shifts defined by the unphosphorylated low-activity state and the mono-phosphorylated (pY657) active state. Furthermore, the assigned chemical shifts of the most active mutant kinase, namely Lys659Glu, are the closest to those of the mono-phosphorylated kinase, FGFR2K^{pY657}, whereas the assigned chemical shifts of the least active mutant kinase, namely Lys659Thr, are the closest to those of the unphosphorylated WT kinase (Figure 4A). This spectral behavior of these pathogenic kinases strongly suggests that these mutants differentially sample a common equilibrium between a structural state resembling the unphosphorylated inhibited state and another resembling the A loop phosphorylated active state. Based on the positions of NMR chemical shifts for the five pathogenic kinases, and on the assumption that the unphosphorylated and A loop phosphorylated FGFR2 kinases represent the pure ground state and the active state, respectively, in a fast two-state conformational exchange regime, the fractional population of kinase molecules occupying the active state was calculated for each mutant (Figure 4B). This approach has been previously used to study the impact of engineered gain- and loss-of-function mutations on the fractional populations of nitrogen regulatory protein C (NtrC) (Volkman et al., 2001) and guanine nucleotide exchange factor Vav1 (Li et al., 2008) in the active state. Using the populations derived from Figure 4B and the normalized activity values from Figure 1B, a quantitative correlation plot was constructed (Figure 4C). The strong correlation (r^2 = 0.97) reveals a direct relationship between an increase in population of kinase molecules in the active state and the degree of gain of function. These data support the two-state model and show that the pathogenic mutations act by altering the intrinsic

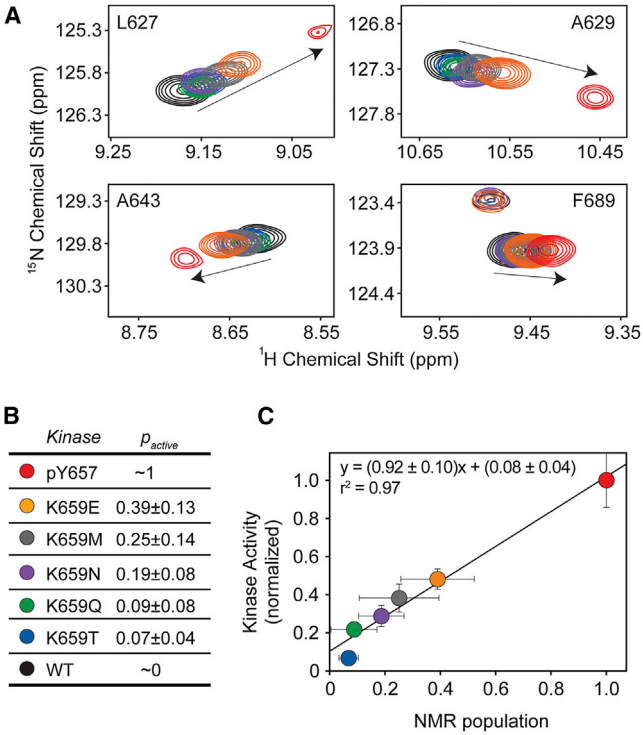

Figure 4. NMR Chemical Shift Spectra for the Unphosphorylated WT FGFR2 Kinase, Unphosphorylated Pathogenic FGFR2 Kinases, and Mono-Phosphorylated FGFR2K^{pY657}

(A) Selected peaks in the [^{1}H,^{15}N] HSQC spectra showing linear chemical shift changes.

(B) The population of active state for each mutant, assuming that the unphosphorylated WT FGFR2 kinase and the mono-phosphorylated FGFR2K^{pY657} respectively represent the pure basal and active states in a fast two-state conformational exchange regime.

(C) Correlation plot of the normalized kinase activity versus the active state population calculated from the NMR chemical shifts. The NMR spectra and correlation plot are color coded for each sample as indicated in (B).

See also Figures S4 and S5.

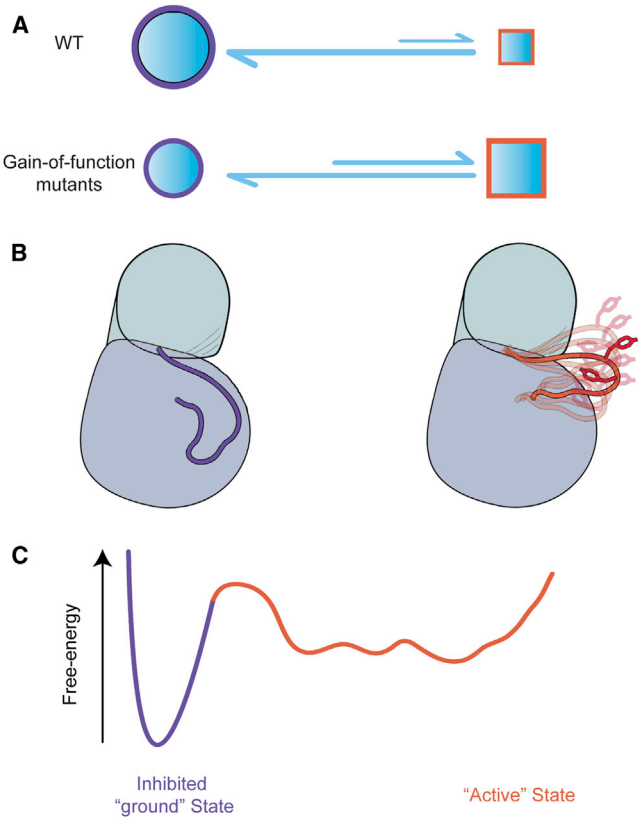

Figure 5. A Two-State Dynamic Equilibrium Model for FGFR Kinase Regulation Deduced from the Structural and Biochemical Data Generated in This Study

In this model, FGFR kinase toggles between an "inhibited" and conformationally rigid ground state, and a more dynamic and heterogeneous "active" state.

(A) Under physiological conditions, FGFR kinases primarily populate the inhibited ground state with only a small fraction of kinases capable of adopting the active state. The pathogenic gain-of-function mutations enable the kinase to more readily attain and reside longer in the active state, thus increasing the overall population of the kinases in the active state. According to this model, the more activating the mutation is, the more the equilibrium is skewed toward the active state. This model explains the molecular basis of the correlation between the degree of gain of function and the severity of clinical manifestation associated with these mutations.

(B) Compared to the structurally rigid kinases in the inhibited ground state, the active state kinases are conformationally more dynamic.

(C) Consistent with the conformational heterogeneity within the active state, kinases in the active state are in the rugged elevated energy state, whereas the kinases in the ground state are in the low-resting energy state.

See also Figures S5, S6, and S7.

conformational dynamics of the kinase to favor the active state (Figure 5).

Free-Energy Landscape of FGFR Kinase Is Biased Toward the Inactive State

Interestingly, the HSQC spectrum of the A loop phosphorylated kinase shows broader peaks for several residues within the catalytic loop that display linear chemical shift changes in the mutated kinases (Figure S5). This spectral behavior implies that compared with the inactive state, the active state is more dynamic (Figure 5B). Consistent with this observation, ^{15}N{^{1}H} R_2 NMR spin relaxation data on the unphosphorylated WT kinase, the pY657 mono-phosphorylated kinase, and unphosphorylated mutant kinases revealed that, akin to A loop phosphorylation, the gain-of-function mutations lead to increases in R_2 consistent with greater conformational flexibility (Figure S6). Taken together, these findings suggest the presence of conformational heterogeneity in the active state arising from an elevated energy landscape compared with the low-energy state of the kinases in the ground state (Figure 5C). The high level of free-energy associated with the active state is harmonious with the fact that the unphosphorylated WT kinase has never been crystallized in the active state and suggests that the gain-of-function mutations cause an increase in the population of active state molecules that is sufficient to enable crystallization of the kinase in the active state. The instability of the active state also explains why the isolated phosphorylated FGFR kinase tends to dephosphorylate over time (H.C. and M.M., unpublished data).

Notably, the two-state model underlying FGFR kinase regulation differs from the conventional two-basin free-energy landscape model proposed for Src and CDK2 kinases (Banavali and Roux, 2009; Berteotti et al., 2009), in which the active state forms a well-defined low-energy basin that is separated by a high-energy barrier from the inactive state (high-energy basin) (Figure S7A). However, our findings are concordant with the NMR spectroscopy and MD simulation data showing that the phosphorylated *apo* form of protein kinase A exists in a "dynamically uncommitted state" characterized by the presence of inhomogeneous line broadening in several loops (Masterson et al., 2011). In the case of the EGFR kinase, molecular dynamics simulation experiments have led to the postulation of a distinct three-state energy landscape model in which a third "disordered" state forms a low-energy basin intervening between the inactive and active states (Shan et al., 2012) (Figure S7B). Similar to the FGFR kinase, the active state of the EGFR kinase also possesses a higher level of free-energy and lacks the typical energy basins seen in Src and CDK2 kinases.

Concluding Remarks

Our X-ray crystallographic and NMR data reveal a direct correlation between gradations of intrinsic kinase activity and a shift in the equilibrium toward the active conformation of the kinase, thus demonstrating that the fractional population of enzyme in an activated state determines the intrinsic activity. We suggest that the two-state dynamic equilibrium model, uncovered here for the regulation of the class IV FGFR kinase family, is also applicable to kinases of the class III RTK subfamily. The three constituents of the molecular brake are fully conserved in class III RTKs, namely PDGFRs, C-KIT, C-FMS, and VEGFRs. In addition, molecular brake mutations in PDGFR and VEGFR also lead to receptor activation and human malignancies (Corless et al., 2005; Medeiros et al., 2004). Moreover, selective ATP-competitive inhibitors of VEGFR and PDGFR often cross-inhibit FGFR kinases (Renhowe et al., 2009), and pathogenic activating mutations in class III RTKs, when grafted into FGFR kinases, confer gain of function (M.M., unpublished data). In conclusion, our data demonstrate that pathogenic mutations act by corrupting the intrinsic conformational dynamics of the kinase to favor the active state, and allow us to draw an elegant correlation between the increase in population of RTK molecules in the active state and the degree of severity in clinical phenotype. In addition to underscoring the importance of tightly controlled regulation of intrinsic RTK activity in human biology, our data provide frameworks for the rational design of inhibitors to tame these hyperactive pathogenic FGFRs for treating human diseases. Finally, our data inform us of innovative strategies for better clinical management of human skeletal disorders by suggesting that the dosage of inhibitors should be adjusted to the degree by which mutations push the kinase into the active conformation.

EXPERIMENTAL PROCEDURES

Protein Expression, Purification, and Crystallization

The cDNA fragments encoding residues Pro449 to Glu759 of human FGFR3c (accession code P22607-1) and Pro458 to Glu768 of human FGFR2c (accession code P21802-1) were amplified by PCR and subcloned into a pET bacterial expression vector with an NH_2-terminal 6×his tag to aid in protein purification. All the mutations were introduced using the QuikChange Site-Directed Mutagenesis Kit (Stratagene). The bacterial strain BL21(DE3) cells were transformed with the expression constructs, and kinase expression was induced with 1 mM isopropyl-L-thio-B-D-galactopyranoside overnight at 16°C–25°C depending on the construct. The cells were lysed, and the soluble kinase proteins were purified according to the published protocol (Chen et al., 2007). Traces of phosphorylation on WT and mutant kinases were removed by treating the proteins with FastAP Thermosensitive Alkaline Phosphatase (Thermo Scientific) and the kinases were repurified by anion exchange chromatography (Mono Q; GE Healthcare Life Sciences). The FGFR2 kinase constructs contain five tyrosine autophosphorylation sites, namely Tyr466 in the juxtamembrane region, Tyr586 and Tyr588 in the kinase insert, and Tyr656 and Tyr657 in the A loop. Of these, phosphorylation on the A loop Tyr657 is sufficient for kinase activation. Because making large quantities of homogeneously penta-phosphorylated FGFR2 kinase sample proved to be challenging, Tyr466, Tyr586, Tyr588, and Tyr656 were mutated to the corresponding nonphosphorylatable residues in FGFR4 kinases (Tyr586Leu and Tyr588Pro) or phenylalanine (Tyr466Phe and Tyr656Phe). This construct ($FGFR2K^{Y657}$) was purified in the same fashion as the WT FGFR2 kinase construct and was phosphorylated on Tyr657 by incubating it with ATP and $MgCl_2$. The homogeneously mono-phosphorylated kinase ($FGFR2K^{pY657}$) was isolated by size exclusion chromatography followed by anion exchange chromatography. N-terminally His-tagged substrate peptide consisting of residues Leu761 to Thr821 of FGFR2c was expressed and purified using sequential Ni^{2+} chelating and size exclusion chromatographies. The substrate peptide corresponds to the C-terminal tail of FGFR2 and contains five authentic tyrosine phosphorylation sites: Tyr769, Tyr779, Tyr783, Tyr805, and Tyr812. Isotopically labeled WT and pathogenic kinases were expressed and purified similar to their unlabeled counterparts.

Protein Crystallization

The purified FGFR2 kinase mutants were concentrated to about 10–100 mg/ml using Amicon Ultra-4 10K Centrifugal Filters (Millipore). Prior to crystallization, the pathogenic kinases were mixed with ATP analog (AMP-PCP) and $MgCl_2$ at a molar ratio of 1:3:15. Initial crystals of pathogenic kinases were grown by hanging drop vapor diffusion at 20°C using crystallization buffer composed of 25 mM HEPES (pH 7.5), 15%–25% w/v PEG4000, 0.2–0.3 M NH_4SO_3, and were further optimized by appropriate additives.

X-Ray Data Collection and Structure Determination

Diffraction data were collected on single cryo-cooled crystals at beamlines X-4A and X-4C at the National Synchrotron Light Source, Brookhaven National Laboratory. Crystals were stabilized in mother liquor by stepwise increasing glycerol concentration to 20% and then flash-frozen in liquid nitrogen. All diffraction data were processed using HKL2000 Suite (Otwinowski and Minor, 1997). Molecular replacement solutions were obtained with AMoRe (Navaza, 1994) using the FGFR2 kinase structure (PDB 2PVY; Chen et al., 2007) as the search model. Rigid body refinements of the mutant kinases were performed using the Crystallography & NMR System (Brünger et al., 1998) by treating the N lobe and C lobe of the kinases as two separate entities. Model building was carried out using O (Jones et al., 1991), and iterative positional and B factor refinements were completed using the Crystallography & NMR System (Brünger et al., 1998) or PHENIX (Adams et al., 2010). Tight noncrystallographic restraints were applied throughout the refinement cycles. Atomic superimpositions were made using lsqkab (Kabsch, 1976) in the CCP4 Suite (Collaborative Computational Project, Number 4, 1994), and structural representations were prepared using PyMOL (DeLano, 2002).

Kinase Assay

Unphosphorylated WT, mono-phosphorylated $FGFR2K^{pY657}$, and unphosphorylated pathogenic FGFR3 and FGFR2 kinases were mixed with kinase reaction buffer containing ATP, $MgCl_2$, and the substrate peptide to the final concentrations of 13.5 μM (kinase), 262 μM (substrate), 10 mM (ATP), and 20 mM ($MgCl_2$). The reactions were quenched at different time points by adding EDTA to the reaction mix with the final concentration of 33 mM. The

progress of the substrate phosphorylation was monitored by native PAGE, and the phosphate incorporation into the substrate peptide was quantified by time-resolved MALDI-TOF mass spectrometry by comparing signals from phosphorylated and the nonphosphorylated peptides as previously published (Chen et al., 2008).

NMR Spectroscopy

The [^{1}H,^{15}N] HSQC spectrum of unphosphorylated FGFR2 kinase, harboring the Ala648Thr mutation (FGFR2K^{A648T}), was assigned using a triple-labeled [^{2}H,^{13}C,^{15}N] sample at ~200 μM in a buffer consisting of 25 mM HEPES (pH 7.5) and 150 mM NaCl. The rational for using this mutant rather than the WT kinase was that the Ala648Thr, which is a pathogenic loss-of-function mutation, increases the yield of protein expression. No significant chemical shift perturbations were observed between unphosphorylated WT and the Ala648Thr mutant FGFR2 kinases, so that the assignment could be transferred unambiguously. A series of TROSY-based triple-resonance experiments (HNCO, HN(CA)CO, HNCOCACB, and HNCACB) were carried out at ^{1}H-frequencies of 800 MHz using cryogenic probes allowing for the assignment of 81% of the non-Pro ^{1}H-^{15}N amide pairs. To ascertain the accuracy of the assignments, FGFR2K^{A648T} was selectively labeled with ^{15}N-labeled amino acids, including Tyr, Gly, Lys, Leu, Val, Phe, Ile, and Met. To compare the effects of the pathogenic mutations and A loop phosphorylation on the conformational dynamics of the FGFR2 kinase, samples of unphosphorylated WT FGFR2 kinase, mono-phosphorylated FGFR2K^{pY657}, and pathogenic FGFR2 kinases were ^{15}N labeled and prepared at a concentration of ~300 μM. All HSQC spectra were acquired with an 800 MHz spectrometer at 25°C. The assignments were transferred to the unphosphorylated WT, mono-phosphorylated FGFR2K^{pY657}, and each of the mutant FGFR2 kinases. The most significant perturbations were found to occur along a linear trajectory, and therefore, the transfer of assignment was somewhat analogous to the peak movement in fast exchange for a ligand titration. To quantify the chemical shift perturbations between phosphorylated and unphosphorylated kinases, the combined chemical shift ($\Delta\delta$) was calculated according to Equation 1:

$$\Delta\delta = \sqrt{(0.154\Delta\delta_N)^2 + \Delta\delta_H^2} \qquad \text{(Equation 1)}$$

$\Delta\delta_N$ and $\Delta\delta_H$ are the chemical shift changes between the unphosphorylated and mono-phosphorylated samples for ^{15}N and ^{1}H-nuclei, respectively. The residues displaying resolved linear chemical shift changes among the samples were used to calculate the population of active state for each sample. We assumed that the mono-phosphorylated kinase had an active state population of 1.0, and the unphosphorylated WT sample was a good approximation of the ground state. Based on this, the population of active state (p_{active}) for each mutant was calculated from the chemical shift positions (δ) of the phosphorylated and unphosphorylated samples:

$$p_{active} = \frac{\delta_{mutant} - \delta_{phos}}{\delta_{unphos} - \delta_{phos}} \qquad \text{(Equation 2)}$$

Residues in the αEF and αG helices showed small deviations from the linear chemical shift trend, which were attributed to their proximity to the Lys659 substitutions in the mutants and the phosphorylated Tyr657 in the mono-phosphorylated FGFR2K^{pY657} (Figures 3 and S3).

ACCESSION NUMBERS

The Protein Data Bank (PDB) accession numbers for the coordinates and structure factors of FGFR2 kinases harboring Lys659Asn, Lys659Met, Lys659Glu, Lys659Gln, or Lys659Thr activating mutation reported in this paper are 4J95, 4J96, 4J97, 4J98, and 4J99.

SUPPLEMENTAL INFORMATION

Supplemental Information includes seven figures and one table and can be found with this article online at http://dx.doi.org/10.1016/j.celrep.2013.06.025.

ACKNOWLEDGMENTS

The authors thank Dr. R. Goetz, Messrs. A. Belov, and Y. Liu for reading the manuscript critically and making thoughtful suggestions and Drs. J. Schwanof and R. Abramowitz at National Synchrotron Light Source (NSLS) for their assistance with diffraction data collection. This work was supported by National Institute of Dental and Craniofacial Research (NIDCR) grant DE13686 (to M.M.), National Institute of Neurological Disorders and Stroke (NINDS) grant P30 NS050276 (to T.A.N.), start-up funding from New York University (to N.J.T.), National Natural Science Foundation of China (NSFC) grants 31270789 and 81102486 (to H.C. and Z.H.), and Zhejiang Key Group Project in Scientific Innovation 2010R10042-01 (to X.L. and Z.H.). Beamlines X4A and X4C of NSLS at Brookhaven National Laboratory, a DOE facility, are supported by the New York Structural Biology Center (NYSBC). Facilities at the NYSBC are supported by the following agencies/grants: National Institutes of Health (grants CO6RR015495 and P41GM066354), New York State Office for Science, Technology and Academic Research (NYSTAR), the Keck Foundation, and New York City Economic Development Corporation (NYCEDC).

Received: March 8, 2013
Revised: May 13, 2013
Accepted: June 14, 2013
Published: July 18, 2013

REFERENCES

Adams, P.D., Afonine, P.V., Bunkóczi, G., Chen, V.B., Davis, I.W., Echols, N., Headd, J.J., Hung, L.-W., Kapral, G.J., Grosse-Kunstleve, R.W., et al. (2010). PHENIX: a comprehensive Python-based system for macromolecular structure solution. Acta Crystallogr. D Biol. Crystallogr. *66*, 213–221.

Banavali, N.K., and Roux, B. (2009). Flexibility and charge asymmetry in the activation loop of Src tyrosine kinases. Proteins *74*, 378–389.

Bellus, G.A., McIntosh, I., Smith, E.A., Aylsworth, A.S., Kaitila, I., Horton, W.A., Greenhaw, G.A., Hecht, J.T., and Francomano, C.A. (1995). A recurrent mutation in the tyrosine kinase domain of fibroblast growth factor receptor 3 causes hypochondroplasia. Nat. Genet. *10*, 357–359.

Bellus, G.A., Bamshad, M.J., Przylepa, K.A., Dorst, J., Lee, R.R., Hurko, O., Jabs, E.W., Curry, C.J., Wilcox, W.R., Lachman, R.S., et al. (1999). Severe achondroplasia with developmental delay and acanthosis nigricans (SADDAN): phenotypic analysis of a new skeletal dysplasia caused by a Lys650Met mutation in fibroblast growth factor receptor 3. Am. J. Med. Genet. *85*, 53–65.

Bellus, G.A., Spector, E.B., Speiser, P.W., Weaver, C.A., Garber, A.T., Bryke, C.R., Israel, J., Rosengren, S.S., Webster, M.K., Donoghue, D.J., and Francomano, C.A. (2000). Distinct missense mutations of the FGFR3 lys650 codon modulate receptor kinase activation and the severity of the skeletal dysplasia phenotype. Am. J. Hum. Genet. *67*, 1411–1421.

Berk, D.R., Spector, E.B., and Bayliss, S.J. (2007). Familial acanthosis nigricans due to K650T FGFR3 mutation. Arch. Dermatol. *143*, 1153–1156.

Berteotti, A., Cavalli, A., Branduardi, D., Gervasio, F.L., Recanatini, M., and Parrinello, M. (2009). Protein conformational transitions: the closure mechanism of a kinase explored by atomistic simulations. J. Am. Chem. Soc. *131*, 244–250.

Brünger, A.T., Adams, P.D., Clore, G.M., DeLano, W.L., Gros, P., Grosse-Kunstleve, R.W., Jiang, J.S., Kuszewski, J., Nilges, M., Pannu, N.S., et al. (1998). Crystallography & NMR system: a new software suite for macromolecular structure determination. Acta Crystallogr. D Biol. Crystallogr. *54*, 905–921.

Castro-Feijóo, L., Loidi, L., Vidal, A., Parajes, S., Rosón, E., Alvarez, A., Cabanas, P., Barreiro, J., Alonso, A., Domínguez, F., and Pombo, M. (2008). Hypochondroplasia and Acanthosis nigricans: a new syndrome due to the p.Lys650Thr mutation in the fibroblast growth factor receptor 3 gene? Eur. J. Endocrinol. *159*, 243–249.

Chen, C.P., Chern, S.R., Shih, J.C., Wang, W., Yeh, L.F., Chang, T.Y., and Tzen, C.Y. (2001). Prenatal diagnosis and genetic analysis of type I and type II thanatophoric dysplasia. Prenat. Diagn. *21*, 89–95.

Chen, H., Ma, J., Li, W., Eliseenkova, A.V., Xu, C., Neubert, T.A., Miller, W.T., and Mohammadi, M. (2007). A molecular brake in the kinase hinge region regulates the activity of receptor tyrosine kinases. Mol. Cell *27*, 717–730.

Chen, H., Xu, C.F., Ma, J., Eliseenkova, A.V., Li, W., Pollock, P.M., Pitteloud, N., Miller, W.T., Neubert, T.A., and Mohammadi, M. (2008). A crystallographic snapshot of tyrosine trans-phosphorylation in action. Proc. Natl. Acad. Sci. USA *105*, 19660–19665.

Collaborative Computational Project, Number 4. (1994). The CCP4 suite: programs for protein crystallography. Acta Crystallogr. D Biol. Crystallogr. *50*, 760–763.

Corless, C.L., Schroeder, A., Griffith, D., Town, A., McGreevey, L., Harrell, P., Shiraga, S., Bainbridge, T., Morich, J., and Heinrich, M.C. (2005). PDGFRA mutations in gastrointestinal stromal tumors: frequency, spectrum and in vitro sensitivity to imatinib. J. Clin. Oncol. *23*, 5357–5364.

DeLano, W.L. (2002). The PyMOL Molecular Graphics System, Version 1.5.0.4 (LLC: Schrödinger).

Dutt, A., Salvesen, H.B., Chen, T.H., Ramos, A.H., Onofrio, R.C., Hatton, C., Nicoletti, R., Winckler, W., Grewal, R., Hanna, M., et al. (2008). Drug-sensitive FGFR2 mutations in endometrial carcinoma. Proc. Natl. Acad. Sci. USA *105*, 8713–8717.

Hubbard, S.R. (2002). Autoinhibitory mechanisms in receptor tyrosine kinases. Front. Biosci. *7*, d330–d340.

Hubbard, S.R., and Till, J.H. (2000). Protein tyrosine kinase structure and function. Annu. Rev. Biochem. *69*, 373–398.

Hunter, T. (2000). Signaling—2000 and beyond. Cell *100*, 113–127.

Jones, T.A., Zou, J.Y., Cowan, S.W., and Kjeldgaard, M. (1991). Improved methods for building protein models in electron density maps and the location of errors in these models. Acta Crystallogr. A *47*, 110–119.

Kabsch, W. (1976). A solution for the best rotation to relate two sets of vectors. Acta Crystallogr. A *32*, 922–923.

Kan, S.H., Elanko, N., Johnson, D., Cornejo-Roldan, L., Cook, J., Reich, E.W., Tomkins, S., Verloes, A., Twigg, S.R., Rannan-Eliya, S., et al. (2002). Genomic screening of fibroblast growth-factor receptor 2 reveals a wide spectrum of mutations in patients with syndromic craniosynostosis. Am. J. Hum. Genet. *70*, 472–486.

Lemmon, M.A., and Schlessinger, J. (2010). Cell signaling by receptor tyrosine kinases. Cell *141*, 1117–1134.

Li, P., Martins, I.R., Amarasinghe, G.K., and Rosen, M.K. (2008). Internal dynamics control activation and activity of the autoinhibited Vav DH domain. Nat. Struct. Mol. Biol. *15*, 613–618.

Masterson, L.R., Shi, L., Metcalfe, E., Gao, J., Taylor, S.S., and Veglia, G. (2011). Dynamically committed, uncommitted, and quenched states encoded in protein kinase A revealed by NMR spectroscopy. Proc. Natl. Acad. Sci. USA *108*, 6969–6974.

Medeiros, F., Corless, C.L., Duensing, A., Hornick, J.L., Oliveira, A.M., Heinrich, M.C., Fletcher, J.A., and Fletcher, C.D. (2004). KIT-negative gastrointestinal stromal tumors: proof of concept and therapeutic implications. Am. J. Surg. Pathol. *28*, 889–894.

Navaza, J. (1994). AMoRe: an automated package for molecular replacement. Acta Crystallogr. A *50*, 157–163.

Otwinowski, Z., and Minor, W. (1997). Processing of X-Ray Diffraction Data Collected in Oscillation Mode, *Volume 276* (New York: Academic Press).

Pellicena, P., and Kuriyan, J. (2006). Protein-protein interactions in the allosteric regulation of protein kinases. Curr. Opin. Struct. Biol. *16*, 702–709.

Pollock, P.M., Gartside, M.G., Dejeza, L.C., Powell, M.A., Mallon, M.A., Davies, H., Mohammadi, M., Futreal, P.A., Stratton, M.R., Trent, J.M., and Goodfellow, P.J. (2007). Frequent activating FGFR2 mutations in endometrial carcinomas parallel germline mutations associated with craniosynostosis and skeletal dysplasia syndromes. Oncogene *26*, 7158–7162.

Rajakulendran, T., and Sicheri, F. (2010). Allosteric protein kinase regulation by pseudokinases: insights from STRAD. Sci. Signal. *3*, pe8.

Renhowe, P.A., Pecchi, S., Shafer, C.M., Machajewski, T.D., Jazan, E.M., Taylor, C., Antonios-McCrea, W., McBride, C.M., Frazier, K., Wiesmann, M., et al. (2009). Design, structure-activity relationships and *in vivo* characterization of 4-amino-3-benzimidazol-2-ylhydroquinolin-2-ones: a novel class of receptor tyrosine kinase inhibitors. J. Med. Chem. *52*, 278–292.

Shan, Y., Eastwood, M.P., Zhang, X., Kim, E.T., Arkhipov, A., Dror, R.O., Jumper, J., Kuriyan, J., and Shaw, D.E. (2012). Oncogenic mutations counteract intrinsic disorder in the EGFR kinase and promote receptor dimerization. Cell *149*, 860–870.

Tavormina, P.L., Shiang, R., Thompson, L.M., Zhu, Y.Z., Wilkin, D.J., Lachman, R.S., Wilcox, W.R., Rimoin, D.L., Cohn, D.H., and Wasmuth, J.J. (1995). Thanatophoric dysplasia (types I and II) caused by distinct mutations in fibroblast growth factor receptor 3. Nat. Genet. *9*, 321–328.

Tavormina, P.L., Bellus, G.A., Webster, M.K., Bamshad, M.J., Fraley, A.E., McIntosh, I., Szabo, J., Jiang, W., Jabs, E.W., Wilcox, W.R., et al. (1999). A novel skeletal dysplasia with developmental delay and acanthosis nigricans is caused by a Lys650Met mutation in the fibroblast growth factor receptor 3 gene. Am. J. Hum. Genet. *64*, 722–731.

Vajo, Z., Francomano, C.A., and Wilkin, D.J. (2000). The molecular and genetic basis of fibroblast growth factor receptor 3 disorders: the achondroplasia family of skeletal dysplasias, Muenke craniosynostosis, and Crouzon syndrome with acanthosis nigricans. Endocr. Rev. *21*, 23–39.

Volkman, B.F., Lipson, D., Wemmer, D.E., and Kern, D. (2001). Two-state allosteric behavior in a single-domain signaling protein. Science *291*, 2429–2433.

Webster, M.K., D'Avis, P.Y., Robertson, S.C., and Donoghue, D.J. (1996). Profound ligand-independent kinase activation of fibroblast growth factor receptor 3 by the activation loop mutation responsible for a lethal skeletal dysplasia, thanatophoric dysplasia type II. Mol. Cell. Biol. *16*, 4081–4087.

Wilcox, W.R., Tavormina, P.L., Krakow, D., Kitoh, H., Lachman, R.S., Wasmuth, J.J., Thompson, L.M., and Rimoin, D.L. (1998). Molecular, radiologic, and histopathologic correlations in thanatophoric dysplasia. Am. J. Med. Genet. *78*, 274–281.